10ème **C**ongrès **F**rançais d'**A**coustique

Lyon, 12-16 Avril 2010

Measurement of shock N-waves using optical methods

P. Yuldashev[1,2], M. Averiyanov[2], V. Khokhlova[2], O. Sapozhnikov[2], S. Ollivier[1], P. Blanc-Benon[1]

[1] Laboratoire de Mecanique des Fluides et d'Acoustique, 36 Av Guy De Collongue 69134 Ecully Cedex

[2] Department of Acoustics, MSU, Leninskie Gory, 119991 Moscow, Fédération de Russie, petr@acs366.phys.msu.ru

Accurate measurement of broadband acoustic signals in air, particularly shock N-waves, remains a challenge. Bandwidth of existing microphones typically does not exceed 140 kHz, which results in significant overestimation of the shock rise time. Various optical methods may be used to design acoustic sensors with improved high-frequency response. Two approaches are examined in this work: focused shadowgraphy and Mach-Zehnder interferometry. The shadowgraphy method was applied to measure shock front of a high amplitude spherical N-wave generated by a spark source. The shock was illuminated by 20 ns short pulses of white light from a flash lamp; shadowgrams were captured by a CCD camera. The rise time of the shock was calculated from the shadow using numerical modeling of light propagation through inhomogeneities of refraction index caused by the shock wave. Experimental results were in a good agreement with theoretical predictions of the shock rise time. However, while the shadowgraphy method is simple and provides good resolution of the shock, its sensitivity is insufficient to measure smooth parts of the waveform. More complex optical method based on a Mach-Zehnder interferometer to measure a whole waveform with high resolution was tested theoretically. Comparison of the spectra of the optically measured waveform and acoustic signal obtained with the microphone also gives absolute frequency calibration of the microphone. A distance between the microphone and a light beam can be taken into account using the results of acoustic wave propagation modeling. The combination of optical and acoustic experimental methods and modeling therefore can be used as an effective instrument for aeroacoustic measurements and calibration of broadband microphones.

1 Introduction

Pressure N-waves with durations of the order of tens of microseconds and amplitudes of 1-2 kPa can be generated in air by electric sparks [1]. Such N-waves have been extensively used in downscaled laboratory experiments on sonic boom propagation in order to study the distortion of N-waves by atmosphere inhomogeneities [2, 3].

The validity of experimental data analysis and the validity of comparison between experimental and theoretical data strongly depend on the accurate knowledge of the initial N-wave parameters such as peak pressure, duration, and shock rise time. It is thus of utmost importance to accurately measure and model the propagation of N-waves in homogeneous air before investigating more complex configurations. However, it has been shown that it is technically difficult to resolve the fine structure of the shocks that have rise times less than one microsecond, mainly because of the limited frequency bandwidth of commercially available microphones.

Additional difficulties of interpretation of N-waves measurements are due to a lack of information provided by manufacturer on the sensitivity, amplitude and phase frequency responses of microphones. Sensitivity of microphones often does not correspond to manufacturer datasheets and varies strongly (2 times and larger). An amplitude response is usually provided without phase response. Strong change in microphone characteristics occurs when the microphone is used in a special environments, like a baffle to avoid influence of diffraction effects on the edges of microphones. In this case the microphone response can differ strongly from the one provided provided by manufacturer for standard exploitation conditions. These difficulties motivates development of a reliable calibration procedure that can be realized in laboratory environment.

Most simply the microphones can be calibrated using only acoustical measurements of spherically divergent N-wave [1, 2, 4, 5]. This method is based on nonlinear lengthening of a finite amplitude wave. Commonly the weak shock theory is applied to describe the N-wave propagation [1, 2]. Recently, the relative roles of nonlinear effects, thermoviscous absorption, and molecular relaxation in N-waveform distortion were studied both experimentally and theoretically [4, 5]. A numerical model based on the generalized Burgers equation was developed and the ability of the model to predict peak pressures and duration of the wave was established. The modeling permits to describe the propagation of N-waves more accurately than the weak shock theory. In contrast to other papers [1, 2], the duration of the pulse is estimated from the spectrum of the wave rather than from the waveform itself. The spectrum method permits to recover N-wave duration even if high frequency content of the spectrum of the N-wave is cut off by the microphone.

However, strong discrepancies between modeling and measurement were observed in estimation of the front shock rise time which was attributed to the limited

bandwidth of the microphone. Also, the acoustical method is not so accurate, since it assumes that the initial N-wave is almost symmetrical, which is not always true. Hence, more accurate experimental techniques are necessary to resolve fine shock structure and to provide more information about the N-waveform. Microphone characteristics (sensitivity, amplitude, and phase response) can be then calculated by comparing spectrum of alternatively measured N-wave with the one measured by the microphone.

An alternative approach to measure pressure shocks in a laboratory environment is to use optical methods instead of acoustic microphones. Using optical methods it is possible to reconstruct the spatial variation of the pressure wave with a good resolution [6]. Two approaches are examined in this work: focused shadowgraphy and Mach-Zehnder interferometry. Shadowgraphy is successfully applied to measure the front shock rise time. Experimental results are presented and compared to theoretical modeling of acoustic wave. Mach-Zehnder interferometry method, intended to measure both the shocks and smooth pressure variations, is analyzed theoretically.

2 Measurement of the shock rise time using shadowgraphy

Among numerous visualization methods for compressible flows (schlieren, interferometry, etc.), the shadowgraphy technique [6] is relatively simple in design but still sufficiently sensitive to obtain images of the acoustic shock wavefront. According to this method the distribution of light intensity in space is photographed and then analyzed. The pattern of the light intensity is formed due to the light refraction on inhomogeneities of the refraction index caused by variations of medium density. Shadow images called *shadowgrams* are captured by a camera at some distance from the shock wave by changing the position of the lens focal plane. Shadowgrams are interpreted by comparison with simulation of light propagation through the inhomogeneity of the refraction index induced by the front shock of the N-wave. In this way, the front shock thickness and its rise time can be obtained.

2.1 Experimental arrangement for acoustical and optical measurements

The experimental setup designed for acoustical and optical measurements of spark-generated N-waves in homogeneous air is presented in Fig. 1. High amplitude pressure pulses are produced by a 15 kV spark source (1) with 15 mm gap between tungsten electrodes. The repetition rate is of the order of 1 Hz. Spherically diverging pulses are measured along the x coordinate with a broadband microphone (Brüel & Kjær, 1/8" diameter, type 4138) coupled with an adapted preamplifier (B&K 2670) and amplifier (B&K Nexus amplifier with extended bandwidth −3 dB at 200 kHz). The microphone is mounted into a baffle (2) in order to avoid diffraction effects on its edge. The recorded signal is digitized (12 bit, 5 MHz) using a data acquisition card (National Instruments PCI 6610). The measurements are performed at increasing source-microphone distances from 15.8 cm to 105 cm. Acoustical measurement results where used to determine the N-wave amplitude and duration and deduce theoretical rise time using a Generalized Burgers equation [4, 5]. Optical equipment includes a flash-lamp (3) (Nanolite KL–L model, 3.5 kV tension), light filter, lens (4) (4 cm diameter, 16 cm focal length), a digital CCD camera (5) (Dantec dynamics, FlowSense 2M) with acquisition system, Nikon lens (6) with 60 mm focal length, and calibration grid. Optical equipment is mounted on a rail and aligned coaxially. The flash-lamp generates short duration (20 ns) light flashes that allow to have a good resolution of the front shock shadow. The focusing lens is used to collimate the flash light in order to have a parallel light beam. The dimension of the CCD camera is 1600 pixels along the horizontal coordinate and 1186 pixels along the vertical coordinate. The lens is used to focus the camera at a given observation plane perpendicular to the optical axis.

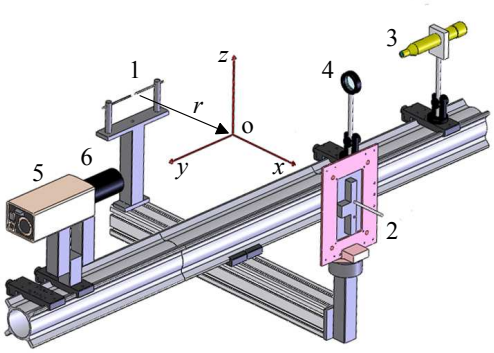

Figure 1: Experimental setup: 1-spark source, 2-microphone in a baffle, 3-Nanolight flash lamp, 4-focusing lens, 5-camera, 6-lens.

Choosing $t = 0$ as the time when a spark is generated, photographs are taken at the instant t when the front shock position is tangent to the optical axis. At this time, a local coordinate system shown in Fig. 1 is defined in the following way: y is the coordinate along the optical axis, which is the light propagation direction from the optical source to the camera; x is the axis in the acoustic source-microphone direction, perpendicular to the optical axis; z is the axis perpendicular to the xy plane. The origin O thus corresponds to the point where the light beam grazes the front shock of the N-wave. The acoustic source coordinates are $(x_S, y_S = 0, z_S = 0)$, with $x_S < 0$. The coordinate r corresponds to the radial distance from the acoustic source, it is related to the local cartesian coordinates by: $r = \sqrt{(x - x_S)^2 + y^2 + z^2}$. The wavefront radius at the observation time t is named R; with this definition $R = |x_S|$. Optical measurements of the shock front are performed for different distances from 15.8 to 65.9 cm between the spark source and the optical axis.

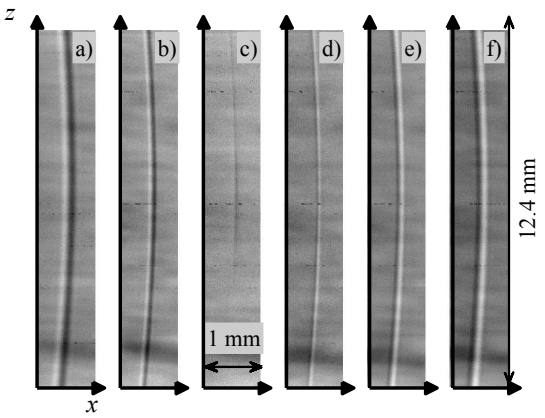

Figure 2: Shadowgrams captured at different positions of observation plane along the light propagation path y = 32 mm (a), 12 mm (b), 2 mm (c), -4 mm (d), -13 mm (e), and -24 mm (f).

2.2 Measurement of shadowgrams

Six photographs of the shock that recorded for the acoustic source-optical axis distance $|x_S| = 15.8$ cm are shown in Fig.2(a-f). The shadowgrams correspond to six different positions of the focal plane of the camera on the y-axis: y = 32 (a), 12 (b), 2 (c), -4 (d), -13 (e), -24 (f) mm. The dimensions of each image are 1 mm (97 pixels) in x direction and 12.4 mm (1186 pixels) in z direction; image scale is 0.0104 mm per pixel. To quantify the width of the shadow of the front shock, the following image processing is applied: 1) spherical curvature of the shock shadow is compensated in order to obtain straight vertical stripes, 2) 2D images with vertical stripes are averaged along the z direction to obtain the variation of light intensity along the x-axis, 3) background noise intensity is estimated and subtracted from the signal. *Shadow width* is defined then as the distance Δx between maximum and minimum values of the light intensity distribution. The shadow width Δx is related to the front shock thickness, which is equal to $c_0\tau_{sh}$, and thus is also related to the rise time τ_{sh}.

2.3 Calculation of the rise time from shadowgrams

In order to establish the relation between the shadow width Δx and the shock thickness $c_0\tau_{sh}$, propagation of light through the inhomogeneity of refraction index induced by the pressure shock is simulated. Acoustic pressure p can be related to the perturbations of the refraction index n of the light by the Eq.1:

$$n = n_0 + k\frac{p}{c_0^2} \qquad (1)$$

Here n_0 is the refraction index of ambient air, c_0 – sound speed, and $k = 0.00023$ m^3/kg is Gladstone-Dale constant [6]. Spatial variations of the refraction index $n - n_0$ around the front shock of the acoustic wave are plotted in Fig. 3. $\Delta n_{sh} = kp_{\max}/c_0^2$ is the magnitude of the refraction index variations for the shock with peak pressure $p_{\max}$. This picture is calculated using the shock with following parameters: $R = 15.8$ cm, $\tau_{sh} = 0.15$ μs,

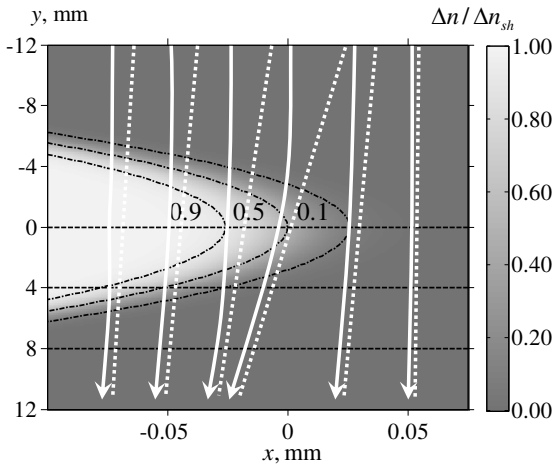

Figure 3: Formation of shadows. Spatial variations of refraction index caused by the acoustic shock front in the xOy plane. Contour dash-dot lines show refraction index levels corresponding to values $0.1\Delta n_{\rm sh}$, $0.5\Delta n_{\rm sh}$ $0.9\Delta n_{\rm sh}$. Refraction of optic rays is schematically shown by arrows (solid lines), back propagation of rays is shown by dashed lines.

$p_{\max} = 1400$ Pa. Refraction of the light is schematically shown by bending arrows.

The light propagation model is based on the parabolic approximation of scalar diffraction theory [7]. For the harmonic wave propagation the equation has the form:

$$\frac{\partial E}{\partial y} = \frac{i}{2k_0}\frac{\partial^2 E}{\partial x^2} + \frac{i\Delta n(x,y)}{n_0}k_0 E \qquad (2)$$

Here $\Delta n(x,y) = n(x,y) - n_0$ is the variation of the refraction index, E is the electric component of the light, $k_0 = 2\pi/\lambda$ is the wave number, λ is the light wavelength, i is the imaginary unit. Equation 2 is solved in finite differences using an operator splitting procedure [8].

The rise time of the front shock is deduced from the images by fitting the shadow width in the image and in the results of the diffraction model. In Fig. 4, the front shock rise time deduced from the optical method and the prediction of the wave propagation model are compared [4]. There is a very good agreement between the results obtained in acoustic modeling and measured optically. The rise times deduced from the experiments are slightly higher than those predicted by the Burgers equation, but the relative error does not exceed 10 %. This result confirms that the rise time of the front shock is much smaller than it could be deduced on the basis of the microphone output voltage.

While being successfully applied to measure the front shock, shadowgraphy appeared to be not sufficiently sensitive to detect the rear shock of the acoustic pulse. One explanation could be that the rear shock is smoother than the front shock due to relaxation effects and diffraction on the spark source electrodes. To measure the rear shock with precision using optical methods, a more sensitive experimental setup should be developed.

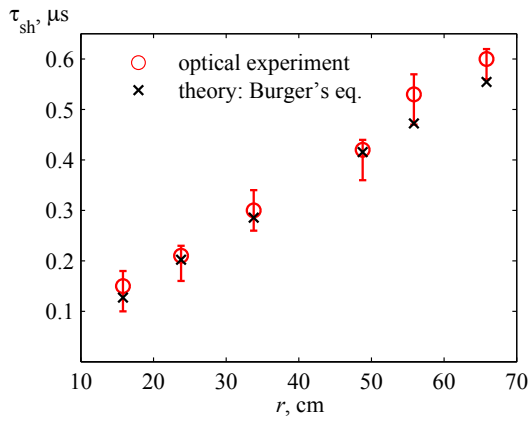

Figure 4: Comparison between the optically measured rise time (circles) and the rise time predicted by using the acoustic wave propagation (crosses) at different distances from the spark source.

3 Mach-Zehnder interferometer as a microphone

Laser interferometry is much more sensitive method in comparison to shadowgraphy. Smeets showed that a Mach-Zehnder interferometer can be used as a point microphone to measure shock waves [9]. Small portion of optical path equal to few millimeters in one of two branches was exposed to acoustic wave. Other parts of the probe beam were protected by conical tubes. The laser beam was focused to 0.1 mm diameter in the test path and was arranged tangent to the wave front of acoustic wave. After bringing beams together light intensity variations were detected by two photodiodes. One of two mirrors was installed on a piezoelectric translator to stabilize the interferometer. The piezoelectrical translator was governed by feedback from intensity signal.

Despite successful results of shock waves measurements shown in [9], some shortcomings call to analyze this experimental method more carefully. First, reflections from edges of the protection tubes can distort rear parts of acoustic wave, that complicates interpretation of the measured signal. In the present paper, to avoid perturbations of incident waves, it is proposed to establish a whole probe beam to acoustical wave with spherical wavefront. Due to sphericity of the wavefront an Abel inversion could be applied to reconstruct the waveform. Second, a time resolution limitations imposed by the beam width, which also varies along light propagation path, should be analyzed. Here the time resolution is obtained using the light propagation modeling through refraction index inhomogeneities induced be the acoustic wave.

3.1 A propagation of a light beam through the N-wave

In a present theoretical investigation the same 2D geometry as in shadowgraphy modeling (see sec. 2.3), is used. A focused Gaussian beam is chosen as a probe beam. The beam propagates along the y axis from negative to positive direction as shown in Fig.5. To simplify the modeling, the spherical N-wave is considered as a "frozen" refraction index inhomogeneity. The light beam is translated along the x-axis to obtain interferometer signal. This scan process is quite different from the actual situation: in experiment the beam is fixed in space and the N-wave passes through it. However, since N-wave length is much lower than the radius of curvature and the N-waveform does not significantly change while propagating at a distance equal to its wavelength, this approximation is applicable.

The beam has a focal length $F = 150$ mm, wavelength $\lambda = 500$ nm. The light propagates from $y = -F$ to $y = F$. Simulations were performed with several initial widths a_0: 100, 250, and 500 μm. Corresponding minimal beam widths $a_{\min} = a_0/\sqrt{z_d^2/F^2 + 1}$ are equal to 92, 89, and 48 μm. Here $z_d = \pi a_0^2/\lambda$ is a diffraction length. The first width a_0 corresponds to almost divergent beam, the last two – to well focused beams.

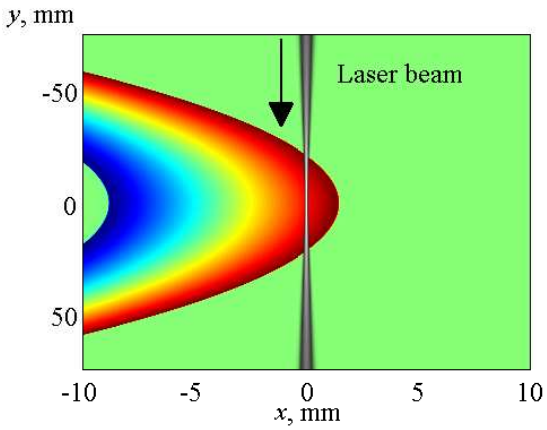

Figure 5: Propagation of Gaussian probe beam through spatial variations of refraction index induced by the N-wave. Amplitude of the beam is shown in gray, refraction index variations are represented in color.

3.2 Treatment of intensity signals

The optical fields of free propagated and probe beams were brought together in the $y = F$ plane. It is supposed later, that intensity is integrated across a surface of photodiodes. The output signal of photodiodes is usually proportional to intensity. The optical phase difference is related to intensity signal by Eq.3 [9]:

$$\sin \Delta\varphi = -\frac{S_1 - S_2}{4\sqrt{I_1 I_2}} \tag{3}$$

Here S_1 and S_2 are averaged intensities of interfered beams,

$$S_1 = \int_{-\infty}^{\infty} |E_1 + E_2|^2 dy \tag{4}$$

$$S_2 = \int_{-\infty}^{\infty} |E_1 - E_2|^2 dy \tag{5}$$

and

$$I_j = \int_{-\infty}^{\infty} |E_j|^2 dx, \; j = 1, 2 \tag{6}$$

are intensities of each of the beams if the second beam is absent.

The variables E_1 and E_2 are the optical fields of reference and probe beams, respectively. The phase difference ψ between two beams consists of optical phase difference $\Delta\varphi$ and a $\pi/2$ factor: $\psi = \Delta\varphi + \pi/2$. This additional phase $\pi/2$ is automatically set by the feedback of a piezoelectric translator, so if the probe beam is not disturbed, i.e. $\varphi = 0$, photodiodes signals are equal $S_1 = S_2$. The Eq.3 is an exact solution that follows from the ray theory. However, as it will be shown in later sections, it is sufficiently accurate for diffractive beams too.

3.3 Magnitude of optical phase difference

To estimate the phase difference induced by the acoustic wave, Eq.(7) can be used.

$$\Delta\varphi = 2\pi \frac{k p_{\max} L}{c_0^2 \lambda} \tag{7}$$

The phase difference is proportional to the peak pressure $p_{\max}$ (amplitude) and to the optical path L in the volume occupied by the acoustic wave in space. For the spherical wave, approximately, $L = \sqrt{2dR}$. Here $d = c_0 T$ is the acoustical wave length, (T is the period or duration), and R is the radius of curvature. For a set of values $p_{\max} = 1500$ Pa, $T = 15$ μs, $R = 15$ cm, the optical path difference is equal $\lambda\Delta\varphi/2\pi = 0.23\lambda$ that can be easily measured [9].

3.4 Reconstruction of the N-waveform from optical phase response

A spherical N-wave with amplitude 1500 Pa, half duration 15 μs, and rise time 0.15 μs was used in numerical simulations as a test wave. Assumption about sphericity of the wave front is crucial for further reconstruction procedure. The beam was moved along the x-axis with a step 8 μm. The phase signal in a case of $a_0 = 250$ μm is shown in the Fig.6 in red. The phase, integrated along a infinitely thin rays, passing the same N-wave, is illustrated by the black line. Actually, this phase is result of a direct Abel transform, that described by Eq.8

$$\Delta\varphi(x) = \frac{2\pi}{\lambda} \int_{x+R}^{+\infty} \frac{2(n(r) - n_0) r dr}{\sqrt{r^2 - (x+R)^2}} \tag{8}$$

Here $n(x, y) = n(r = \sqrt{(x+R)^2 + y^2})$ is a spatial distribution of refraction index. As will readily be observed, in general there is not significant difference between ray theory and simulation of diffracted beam, so the signal of the beam was calculated correctly. Reconstruction of the one dimensional distribution of the wave pressure along the x axis is accomplished using Abel inversion Eq.9:

$$n(r) - n_0 = -\frac{\lambda}{2\pi} \frac{1}{\pi} \int_{r}^{+\infty} \frac{d\Delta\varphi(x+R)}{dx} \frac{dx}{\sqrt{(x+R)^2 - r^2}} \tag{9}$$

A Fourier-Hankel method was used in a numerical evaluation of Eq.9 [10]. The algorithm was tested by reconstructing the signal of direct Abel transform. The error was lower than 0.05 %.

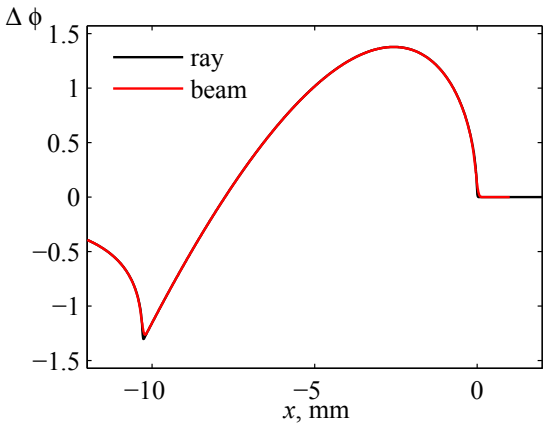

Figure 6: Optical phase difference of the beams modeled using parabolic approximation (red line) and traced along straight rays (black line)

3.5 Results

The results of reconstruction of the test N-wave (black line) are presented in a Fig.7. Different beam widths a_0 are marked by colors: red – 100 μm, green – 250 μm and blue – 500 μm. It is seen, that for all a_0 the linear trend between front and rear shocks of the N-wave is perfectly reconstructed (Fig.7a). A zoom of the reconstructed waveforms near the front shock is presented in the Fig.7b. The front shock is slightly smoothed. The rear shock behaves similarly. Shock smoothing is the effects of averaging of the optical phase across beam width. The rise times, deduced from reconstructed waveforms are listed in a Table 1. A focal beam widths $a_{\min}$ are also presented.

a_0, μm	$a_{\min}$, μm	τ_{sh}, μs
100	98	0.88
250	89	0.38
500	48	0.23

Table 1: The rise time τ_{sh} of reconstructed waveforms for different beam widths a_0

It is seen, that interferometer can achieve submicrosecond time resolution, that is unattainable for standard acoustic microphones [4]. The finest beam result in highest resolution. For the less strong shocks the effect of time resolution will be less pronounced and almost perfect reconstruction is possible. The other advantage of interferometer method is that it is directly gives acoustical wave pressure, as optical properties of air are well known [9, 6].

4 Summary and conclusion

In order to estimate rise time of the front shock more accurately, optical measurements based on a focused shad-

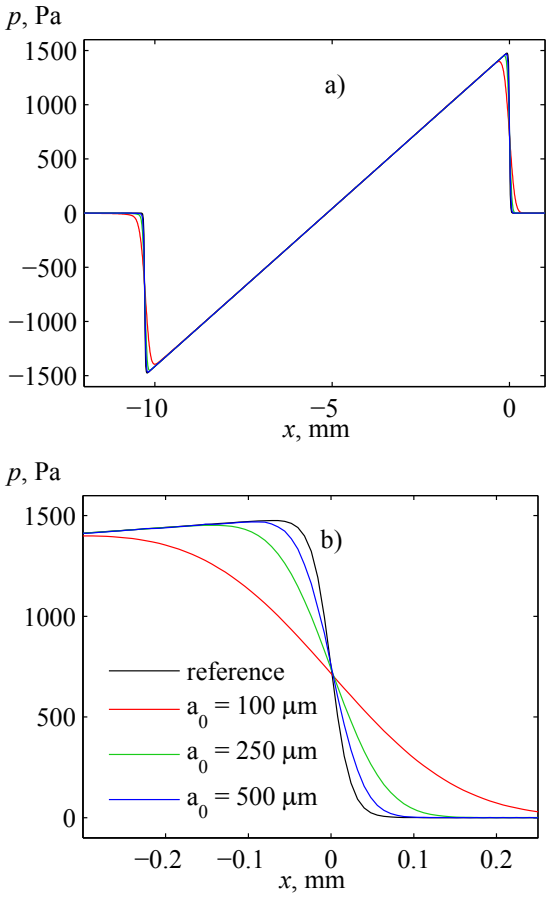

Figure 7: Comparison of reference N-waveform (black line) with waveforms reconstructed from the phase difference of Gaussian beams with different initial widths: $a_0 = 100\mu m$ (red line), $250\mu m$ (green line) and $500\mu m$ (blue line). A whole waveforms (a) and the front shocks (b) are presented.

owgraphy technique are performed. Shock front shadowgrams are captured and analyzed. To interpret shadowgrams, the refraction index inhomogeneity produced by the shock is modeled. The rise times deduced from shadowgrams using the parabolic model are in very good agreement with the acoustic modeling, thus validating the acoustic wave propagation model [4] and the accuracy of the optical measurements

Another optical method with superior precision in comparison to shadowgraphy and based on Mach-Zehnder interferometer is investigated theoretically. Response of the interferometer in a case of Gaussian probe beam and spherical N-wave is simulated using the parabolic model. A time resolution is calculated for different beam widths. It is shown, that a submicrosecond resolution can be achieved in a case of sufficiently fine beam. Opposite to shadowgraphy, interferometer also shows a good results in the low frequency domain (slow pressure variation).

Combination of absolute sensitivity, good resolution at high and low frequencies can be attractive advantages in application of the interferometer in the calibration procedure of acoustical microphones. The acoustical microphone can be placed at some distance (few centimeters) beyond the probe beam along the N-wave propagation path. An evolution of N-wave between the probe beam and the microphone can be taken into account theoretically using Burgers-type equation [4]. Comparison of a spectrum of the waveform recorded by the interferometer and a spectrum of a signal of the microphone will give the frequency response.

Acknowledgments

This work has been partially supported by RFBR and PICS grants. Computer simulations were performed using “Chebyshev” SKIF-MSU computer complex. The authors are grateful to Jean-Michel Perrin for his help with the fabrication of the experimental setup.

References

[1] W. M. Wright, “Propagation in air of N-waves produced by sparks,” *J. Acoust. Soc. Am.*, vol. 73, pp. 1948–1955, 1983.

[2] B. Lipkens and D. T. Blackstock, “Model experiment to study sonic boom propagation through turbulence. Part I: Model experiment and general results,” *J. Acoust. Soc. Am.*, vol. 103, pp. 148–158, Jan. 1998.

[3] S. Ollivier and P. Blanc-Benon, “Model experiment to study acoustic N-wave propagation through turbulence,” in 10^{th} *AIAA/CEAS Aeroacoustics Conference, Manchester,UK*, pp. AIAA2004–2921, May 2004.

[4] P. V. Yuldashev, M. V. Aver’yanov, V. A. Khokhlova, S. Ollivier, and P. Blanc-Benon, “Nonlinear spherically divergent shock waves propagating in a relaxing medium,” *Acoust. Phys.*, vol. 54, pp. 32–41, Jan. 2006.

[5] M. V. Averiyanov, P. V. Yuldashev, V. A. Khokhlova, S. Ollivier, and P. Blanc-Benon, “Nonlinear propagation of spark-generated N-waves in relaxing atmosphere: laboratory-scaled experiments and theoretical study,” in 13^{th} *AIAA/CEAS Aeroacoustics Conference, AIAA-2007-3676*, May 2007.

[6] G. S. Settles, *Schlieren and shadowgraph techniques: visualizing phenomena in transparent media*. Springer-Verlag, Heidelberg, 2001.

[7] J. W. Goodman, *Introduction to Fourier Optics*. 2ed., McGraw-Hill, 1996.

[8] W. F. Ames, *Numerical Methods for Partial Differential Equations*. Academic, San Diego, 3rd ed., 1992.

[9] G. Smeets, “Laser interference microphone for ultrasonics and nonlinear acoustics,” *J. Acoust. Soc. Am.*, vol. 61, pp. 872–875, Mar. 1977.

[10] S. Ma, H. Gao, and L. Wu, “Modified fourier-hankel method based on analysis of errors in abel inversion using fourier transform techniques,” *Appl. Opt.*, vol. 47, no. 9, pp. 1350–1357, 2008.